Geomodeling exam report

Finite difference modeling of flow in a deformable porous medium

Anders Damsgaard
anders.damsgaard@geo.au.dk, https://cs.au.dk/~adc

Last revision: October 29, 2013

Abstract

This document is the exam report for the course "Geomodelling", held by David Lundbek Egholm and Mads Faurschou Knudsen at the Department of Geoscience, Aarhus University, during the spring semester 2013. This report is the result of a self-chosen study subject, and restrained by a 15 page limit. A simple coupling between granular and fluid dynamics is presented, based on macroscopic parameterization and neglect of fluid inertia. The limitations and future steps are discussed.

Contents

1 Introduction **2**
1.1 Mechanics of fluid-saturated granular media 2
1.2 Numerical modeling 2

2 Methods **3**
2.1 Discrete element modeling 3
2.2 Darcy's law 3
2.3 Finite difference method 4
2.4 Numerical implementation 5

3 Results **8**
3.1 Validation of fluid flow 8
3.1.1 Conservation of fluid mass 8
3.1.2 Comparison to an analytical solution of transient flow 9
3.2 Fluid dynamics during granular deformation 10
3.3 Performance 11

4 Outlook **11**

5 Conclusion **14**

References **14**

1 Introduction

The flow of one or more liquid phases through porous media is a widely researched topic, of interest to e.g. oil research, groundwater investigation and petrology research parties.

In this study, I present a one-way coupled methodology between granular particles and a single-phase inter-particle fluid. The particle–fluid multiphase flow is modeled using a Euler–Lagrangian approach. The coupled approach is validated against analytical solutions of porous flow, and demonstrated to simulate fluid pressure and flow dynamics during granular deformation. Afterwards, the implications of the simplifying assumptions in the one-way coupling are considered, along with an outlook on approaches to improve the coupled methodology.

The presented implementation is based on a macroscopic parameterization. When using this approach, the fluid grid cells are large compared to the particles. Consequently, the fluid flow is only resolved to a coarse resolution. Alternatively, the fluid can be simulated by the lattice-Boltzmann method, which requires the discretization of the inter-particle cell space. While this approach results in a better-resolved fluid flow, the computationally requirements are greatly heightened. Zhu and others (2007) review the different techniques of fluid and solid simulation and coupling.

1.1 Mechanics of fluid-saturated granular media

When dry granular materials are in a static or pseudo-static state, their rheology and mechanical properties are rate independent (Nedderman, 1992; Jaeger and others, 1996; GDR-MiDi, 2004).

Under the presence of fluids in the inter-particle void, either in unsaturated (e.g. Richefeu and others, 2006) or saturated conditions (e.g. Iverson and others, 1998), the behavior can become strain dependant due to the fluid viscosity. If the rate of deformation ($\dot{\epsilon}$) is sufficiently high, relative to the hydraulic conductivity (K), the volumetric increase caused by granular deformation (Reynolds, 1885; Mead, 1925), leads to a drop in the local pore fluid pressure. The transient fluid pressure decrease causes an increase of the magnitude of stress carried by the granular skeleton. This strengthens the inter-granular contacts, and causes an overall strain hardening (Iverson and others, 1998). The potential hardening mechanism inside the shear zone could be sufficient to cause shear-zone migration.

The requirement of the proposed mechanism of strain-hardening is volumetric expansion (dilation) of the material in the shear zone. Analog and numerical experiments have shown that angular particles exhibit contraction in the first stage of shear (Li and Aydin, 2010; Damsgaard and others, 2013), which in the same theoretical framework leads to a transient strain softening. This study present the first steps in attempting to numerically quantify the role of internal fluid dynamics upon the behavior of the particle-fluid mixture.

1.2 Numerical modeling

The fluid phase is investigated at the mesoscopic scale, and simulated by an averaged formulation for porous flow in a continuum grid. Gerya (2010) lists the governing partial-differential equations for continuum modeling:

- The equation of continuity (conservation of mass)
- The equation of motion (conservation of momentum – Navier-Stokes equations)
- The temperature equation (conservation of heat)

In the presented implementation, the equation of continuity and a simplified form of the equation of motion are combined to simulate fluid flow in a porous material. Instead of

solving the full Navier-Stokes problem, the fluid is assumed to be incompressible, and the inertial terms are neglected assuming low flow velocities.

Bueler (2012) proposed three techniques that can be used to be certain that an implemented numerical scheme is correct:

1. Don't make any mistakes.
2. Compare the results with others.
3. Compare the numerical results to an exact (analytical) solution.

Method 1 may be the most intuitive way of producing a working implementation. Mistakes during computer programming (*bugs*) are however difficult to avoid, and can be introduced by typing errors, oversights, misunderstandings, etc. There are several types of bugs[1]. Some types are relatively easy to resolve. Modern compilers generally do a good job of warning about typing errors in the programming language keywords. Other types are harder to locate. For this reason, in the numerical implementation presented here, I have relied on method 3. The analytical implementation and its results are verified with method 2.

2 Methods

2.1 Discrete element modeling

The particles are simulated with the Discrete Element Method (DEM) using the soft-body contact model (Cundall and Strack, 1979; Damsgaard and others, 2013). This method explicitly resolves particle interaction based on parameterization of the inter-particle contact mechanics. The particles are represented as spheres, with translational and rotational degrees of freedom. The contact model consists of linear-elastic repulsion upon contact, limited by the frictional strength of the inter-particle interface.

2.2 Darcy's law

Initially empirically constrained, and later derived from the Navier-Stokes equations by neglecting fluid inertia, Henry Darcy's law describes the flow of fluid through a porous medium, driven by a hydraulic pressure gradient. The specific fluid flux q ($\mathrm{m\,s^{-1}}$) can in vector calculus notation be written as

$$\vec{q} = -K\nabla H \tag{1}$$

or along the axes of a three-dimensional Cartesian coordinate system be specified as a set of partial differential equations (Sonnenborg and Henriksen, 2005):

$$q_x = -K_x \frac{\partial H}{\partial x} \qquad q_y = -K_y \frac{\partial H}{\partial y} \qquad q_z = -K_z \frac{\partial H}{\partial z} \tag{2}$$

where H is the *potentiometric* or *hydraulic* head, and K is the hydraulic conductivity ($\mathrm{m\,s^{-1}}$). The hydraulic conductivity is a function of the permeability k ($\mathrm{m^2}$), the fluid density ρ_f ($\mathrm{kg\,m^{-3}}$), the gravitational acceleration g ($\mathrm{m^2\,s^{-1}}$), and the dynamic viscosity of the fluid μ ($\mathrm{Pa\,s}$):

$$K = \frac{k\rho_f g}{\mu} \tag{3}$$

Defining the reference elevation as 0, the hydraulic head is related to the fluid pressure P by $H = P/(\rho_f g)$. Analogous to Fouier's law of heat transfer, the evolution of hydraulic

[1] `http://www.linuxforu.com/2010/10/joy-of-programming-types-of-bugs/`

heads (or hydraulic pressures) in a discretized domain can be considered a problem of conduction. Darcy's law assumes laminar flow at all times. The hydraulic permeability (k) can be estimated from laboratory tests, or from empirical relationships based on e.g. the size of the finest particles (Hazen, 1911; Harleman and others, 1963), the geometric mean diameter (Krumbein and Monk, 1943), or the porosity (Kozeny, 1927). For the purposes here, the hydraulic permeability (k) is estimated as a function of the porosity ϕ (-) and the representative grain diameter (d_m) using the Kozeny-Carman relationship (Kozeny, 1927; Carman, 1937, 1956; Nelson, 1994; Boek and others, 2012):

$$k \approx \frac{\phi^3}{(1-\phi)^2}\left(\frac{d_m^2}{180}\right) \tag{4}$$

In the presented simulations, the particle size distribution is narrow, and the mean grain diameter is used as the representative grain size. Assuming that the pore fluid is an ideal fluid, frictional losses are neglected. The change in pressure at a point in time includes a volumetric flux term W (s^{-1}), that has a negative value if fluid is extracted. By considering the conservation of mass, the change in hydraulic head in a cell equals the net inflow and recharge (Sonnenborg and Henriksen, 2005):

$$S_s\frac{\partial H}{\partial t} = -\frac{\partial q_x}{\partial x} - \frac{\partial q_y}{\partial y} - \frac{\partial q_z}{\partial z} + W \tag{5}$$

where S_s is the specific hydraulic storage (m^{-1}) of the cell, a measure of the amount of water an aquifer volume releases per length change in the hydraulic head. When combining the equations for Darcy flow (eq. 2) with the mass conservation equation (eq. 5), the governing partial differential equation for three-dimensional porous fluid flow is written as:

$$S_s\frac{\partial H}{\partial t} = \frac{\partial}{\partial x}\left(K_x\frac{\partial H}{\partial x}\right) + \frac{\partial}{\partial y}\left(K_y\frac{\partial H}{\partial y}\right) + \frac{\partial}{\partial z}\left(K_z\frac{\partial H}{\partial z}\right) + W \tag{6}$$

or written with the Laplace operator, assuming that the hydraulic conductivity K is anisotropic:

$$\frac{\partial H}{\partial t} = \frac{1}{S_s}\left(K\nabla^2 H + W\right) \tag{7}$$

To incorporate the effect of porosity changes upon the hydraulic pressure, I will replace the volumetric flux term W (s^{-1}) with porosity change (s^{-1}):

$$\frac{\partial H}{\partial t} = \frac{1}{S_s}\left(K\nabla^2 H - \frac{\partial \phi}{\partial t}\right) \tag{8}$$

With this formulation, a porosity increase reduces the hydraulic pressure.

2.3 Finite difference method

The finite difference method is a method used to approximate the solution of a differential equation. The spatial gradient (first order derivative, $f'(x)$) of e.g. the temperature in a solid medium or the pressure in a porous material, is the property determining the rate of temperature conduction or porous fluid flow, respectively. The finite difference method approximates the derivative at a point x by sampling one or more neighboring points, positioned at e.g. $x \pm \Delta x$.

In the case of a decreasing step size ($\Delta x \to 0$), the value of the approximated gradient goes towards the value of the true gradient at x:

$$f'(x) = \lim_{\Delta x \to 0}\frac{f(x+\Delta x) - f(x)}{\Delta x} \tag{9}$$

In numerical computing, the value of Δx is required to be finite. By assuming that the function derivatives can be approximated by Taylor's theorem, the value at a finite distance (Δx) from a point (x) can be found by including the higher order derivatives in the Taylor-series expansion:

$$f(x+\Delta x) = f(x) + \frac{f'(x)}{1!}\Delta x^1 + \frac{f''(x)}{2!}\Delta x^2 + \ldots + \frac{f^{(n)}(x)}{n!}\Delta x^n + R_n(x) \tag{10}$$

Here, $R_n(x)$ is the remainder truncation term when n has a finite value. In order to solve the partial differential equations of porous flow, the first order derivatives need to be determined. The second and higher order factors are omitted, resulting in a total truncation error of $R_1(x)$. Assuming that the error is neglegible ($R_1(x) \approx 0$), the truncated Taylor series becomes the form:

$$f(x+\Delta x) \approx f(x) + \frac{f'(x)}{1!}\Delta x^1 = f(x) + f'(x)\Delta x \tag{11}$$

The first-order derivative ($f'(x)$) is the unknown term, and by rearranging equation 11 it can finally be approximated in the *forward difference* form:

$$f'(x) \approx \frac{f(x+\Delta x) - f(x)}{\Delta x} \tag{12}$$

alternatively in the *backward difference* form:

$$f'(x) \approx \frac{f(x) - f(x-\Delta x)}{\Delta x} \tag{13}$$

or in the *central difference* form:

$$f'(x) \approx \frac{f(x+\Delta x) - f(x-\Delta x)}{2\Delta x} \tag{14}$$

Note that the central difference approximation of the derivative of $f'(x)$ doesn't consider the value $f(x)$, but only at at the neighboring points.

2.4 Numerical implementation

The flow solver was initally written in C++. Once the solver behavior was validated, it was ported to CUDA C (NVIDIA, 2013) for increased performance. The Darcy solver is incorporated into the `sphere`[2] particle dynamics simulator, as a first step towards implementing a two-way coupling between grains and an inter-particle fluid.

The spatial model domain is discretized into a uniform (constant Δx), cubic, three-dimensional grid. Each cell is identified by a unique index i, computed from the three-dimensional grid-coordinate (x, y, z) by:

$$i = x + n_x y + n_x n_y z \tag{15}$$

where n_x, n_y, and n_z are the grid dimensions. In the following, both the i and (x, y, z) notation will be used to identify cells in the grid, depending on what style suits the context.

In a cell i with a set of particles inside ($\mathbf{n}_i$), the cell porosity is found by subtracting the volume of the solid fraction (V_i^s) from the cell volume ($V^c = \Delta x \Delta y \Delta z$):

$$\phi_i = \frac{V^c - V_i^s}{V^c} \tag{16}$$

[2] `https://github.com/anders-dc/sphere`

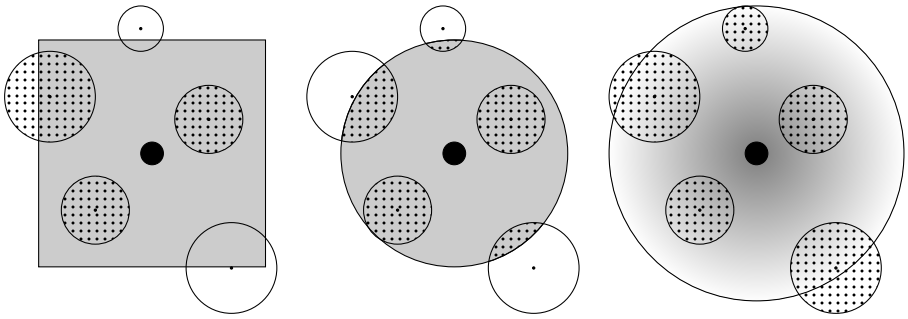

Figure 1: Three methods for determining the porosity in a cell, visualized in two dimensions. The large black dot denotes the cell center (node), the gray shading shows the cell volume V_c, and the dotted areas are the solid volume V_s. (left) Cubic sorting cell-based porosity estimation method, (center) spherical cell volume method, (right) inverse-distance weighted method, where the cutoff distance is distance marked by the large circle.

Since it is difficult to formulate the common volume between a cube and a sphere (potentially a problem of a sphere intersecting with three planes), the particles are binned into cubic cells according to their center position (fig. 1, left), and the entire particle volume contributes to the cell solid volume:

$$V_i^s = \sum_j^{\mathbf{n}} \frac{4}{3}\pi r_j^3 \quad \textit{if } \vec{x}_i < \vec{x}_j < \vec{x}_i + \Delta\vec{x} \tag{17}$$

where $\vec{x}_i$ is the vector pointing towards the cell corner closest to the coordinate system origo, and $\vec{x}_i + \Delta\vec{x}$ is the most distant cell corner. $\vec{x}_j$ is the position of the particle center.

This approximation of cell porosity is untrue for all grid sizes, but converges towards the true value with increasing cell size. Since Darcy's law is a constitutive equation of macroscopic flow, and the cell hydraulic conductivity is an anisotropic quantity, this simplification may be reasonable. In order to avoid numerical errors due to this approximation, the cell porosity values are limited to the interval $]0;1[$. It should be noted that this porosity approximation leads to non-continuous porosity values through time, if particles are moving across cell boundaries.

The solid volume is in the spherical cell volume method (fig. 1, center) determined by the intersection of the spherical cell volume (V_c) and the sum of intersecting particle volumes (V_s). The spherical cell volume has a center at $\vec{x}_i$, and a radius of R_i. The nearby particles are characterized by position $\vec{x}_j$ and radius r_j. The center distance is defined as:

$$d_{ij} = ||\vec{x}_i - \vec{x}_j|| \tag{18}$$

The common volume of the two intersecting spheres is zero if the volumes aren't intersecting, lens shaped if they are intersecting[3], and spherical if the particle is fully contained by the spherical cell volume:

$$V_i^s = \sum_j \begin{cases} 0 & \textit{if } R_i + r_j \leq d_{ij} \\ \frac{1}{12d_{ij}}\left[\pi(R_i + r_j - d_{ij})^2(d_{ij}^2 + 2d_{ij}r_j - 3r_j^2 + 2d_{ij}R_i + 6r_jR_i - 3R_i^2)\right] & \textit{if } R_i - r_j < d_{ij} < R_i + r_j \\ \frac{4}{3}\pi r_j^3 & \textit{if } d_{ij} \leq R_i - r_j \end{cases} \tag{19}$$

The cell sphere will typically have a diameter that is equal to the cell width. Using this method, the cell porosity values are continuous through time as particles enter and exit the cell volume.

[3] `http://mathworld.wolfram.com/Sphere-SphereIntersection.html`

A third possibility of determining the cell volume consists of weighing the effect of a particle upon the porosity based on the inverse distance between the particle and the cell center (fig. 1, right). Using this method, the closer a particle is placed to the cell center, the more important the volume of the particle becomes upon the cell porosity, and the porosity values are continuous through time. The mathematical formulation for this setup hasn't yet been formulated, and will be the focus of a future investigation. In section 3.2 I will compare the first two porosity estimation methods.

Using an explicit integration scheme, the new values of the hydraulic head in a cell at (x, y, z) are found on the basis of the current hydraulic pressure, the gradient magnitudes, and the cell porosity change. The implementation allows for heterogeneous values of transmissivity (i.e. hydraulic conductivity), similar to the finite-difference scheme in the U.S. Geological Survey groundwater flow code MODFLOW[4], and consists of forward and backward differences in the regular, cubic grid:

$$\begin{aligned} H^{t+\Delta t}_{x,y,z} = H^{t}_{x,y,z} + \frac{\Delta t}{S_{x,y,z}} \Bigg[& \frac{T^{-}_{xx}(H_{x-1,y,z} - H_{x,y,z})}{\Delta x^2} + \frac{T^{+}_{xx}(H_{x+1,y,z} - H_{x,y,z})}{\Delta x^2} \\ & + \frac{T^{-}_{yy}(H_{x,y-1,z} - H_{x,y,z})}{\Delta y^2} + \frac{T^{+}_{yy}(H_{x,y+1,z} - H_{x,y,z})}{\Delta y^2} \\ & + \frac{T^{-}_{zz}(H_{x,y,z-1} - H_{x,y,z})}{\Delta z^2} + \frac{T^{+}_{zz}(H_{x,y,z+1} - H_{x,y,z})}{\Delta z^2} \\ & + Q_{x,y,z} - \frac{\Delta\phi\Delta\bar{x}}{\Delta t} \Bigg] \end{aligned} \tag{20}$$

where Q is the local recharge (or source) term ($\mathrm{m\,s^{-1}}$), which can be of negative- or positive value. $\Delta\bar{x}$ is the mean cell width. The new value of H is limited to be within the range $[0; \infty[$ m. The hydraulic transmissivity T ($\mathrm{m^2\,s^{-1}}$) is proportional to the hydraulic conductivity and the cell size:

$$T_x = K_{xx}\Delta x \qquad T_y = K_{yy}\Delta y \qquad T_z = K_{zz}\Delta z \tag{21}$$

The hydraulic transmissivity between a pair of cells of different transmissivities is determined as the harmonic mean, e.g. between a cell (x, y, z) and its neighbor along the positive x-axis direction:

$$T^{+}_{xx} = \frac{2T^{x}_{x,y,z}T^{x}_{x+1,y,z}}{T^{x}_{x,y,z} + T^{x}_{x+1,y,z}} \tag{22}$$

The harmonic mean corresponds to a set of resistors in series, and is a better formulation for the conductive problem between transmissivity contrasts than the arithmetic mean (Sonnenborg and Henriksen, 2005).

The cell hydraulic storativity S_i ($\mathrm{m^2}$), acts as a relaxation parameter (Gerya, 2010), determining how strongly the computed gradients affect the change in hydraulic head. It is calculated from the cell specific storage S^i_s:

$$S_i = S^i_s \Delta x \Delta y \Delta z \tag{23}$$

The usage of an explicit integration scheme imposes strict demands for obtaining numerical stability. To ensure a stable solution, the simulation parameters must fulfill the following criteria (Sonnenborg and Henriksen, 2005; Gerya, 2010):

$$\frac{\max(T)}{\min(S)} \left(\frac{\Delta t}{\Delta x^2} + \frac{\Delta t}{\Delta y^2} + \frac{\Delta t}{\Delta z^2} \right) \leq 0.5 \tag{24}$$

[4] `https://en.wikipedia.org/wiki/MODFLOW`

If the time step on the other hand is too small, the machine floating-point precision will begin to be significant to the magnitude of the gradients in the hydraulic heads, causing a cumulative build up of an arithmetic error.

Implicit integration schemes are generally preferable in terms of numerical stability and time step length (e.g. Gerya, 2010), but the deficit of solvers of systems of equations for the GPU platform caused the explicit solver choice. The Discrete Element operations require very small time steps. The fluid operations are performed once per DEM time step.

The cell fluid-flow velocities are computed on the base of the local specific flux (eq. 2), and the porosity (eq. 16):

$$\vec{v}_i = \frac{\vec{q}_i}{\phi_i} \tag{25}$$

The cell hydraulic flux vector ($\vec{q}_i$) is found using eq. 2, where the hydraulic head gradient is approximated by a first-order central difference scheme and the six nearest neighbors. The diagonal neighbors are not considered. For a cell i at the grid position (x, y, z) with grid spacing Δx, the x-component at time t is approximated by:

$$\frac{\partial H^t_{x,y,z}}{\partial x} \approx \frac{H^t_{x+1,y,z} - H^t_{x-1,y,z}}{2\Delta x} \tag{26}$$

The derivatives of the hydraulic head along the y and z axes are found in a similar way.

The upper and lower boundaries in the presented simulations are no-flow planes, implemented by Neumann boundary conditions. No-flow condition is implemented at e.g. the top boundary by setting the forward difference term in eq. 20 to a value of 0. The cells at the top boundary can still have fluid fluxes in the x, y, and $-z$ directions. The lateral boundaries are periodic. The numerical grid is padded by ghost-nodes to avoid read/write conflicts when computations are performed in parallel.

3 Results

3.1 Validation of fluid flow

3.1.1 Conservation of fluid mass

A first step in ensuring that the numerical diffusion code produces correct results is to check that the fluid mass is conserved through time. This test is analogous to the conservation of heat in a thermal conduction model.

The cells are initialized at uniform values, except of a small perturbation of a different head value. The Kozeny-Carman approximation (eq. 4) is disabled by setting the hydraulic conductivities (K) to a constant, homogeneous value of $1 \times 10^{-2}\,\mathrm{m\,s^{-1}}$. The specific storages (S_s) are set to $1\,\mathrm{m^{-1}}$. The model domain has the spatial dimensions $6.8 \times 6.8 \times 2.1\,\mathrm{m}$, discritized into a grid of the dimensions $(n_x, n_y, n_z) = 32 \times 32 \times 10$. The default hydraulic heads are $1\,\mathrm{m}$, and a perturbation value of $2\,\mathrm{m}$ is inserted at $(i_x, i_y, i_z) = (4, 4, 4)$.

The results in figure 2 show that the perturbation is diffused to the adjacent volumes as a function of time. The perturbation propagates into the neighboring cells, obtains a three-dimensional Gaussian bell shape, before being spatially constrained by the upper and lower boundaries. The color bars denote the minimum and maximum values of the hydraulic heads. The total sum of the hydraulic heads is close to constant. The percent-wise difference between the maximum and minimum value of $\bar{H}$ is $4 \times 10^{-11}\%$, caused by the finite precision in the floating point operations.

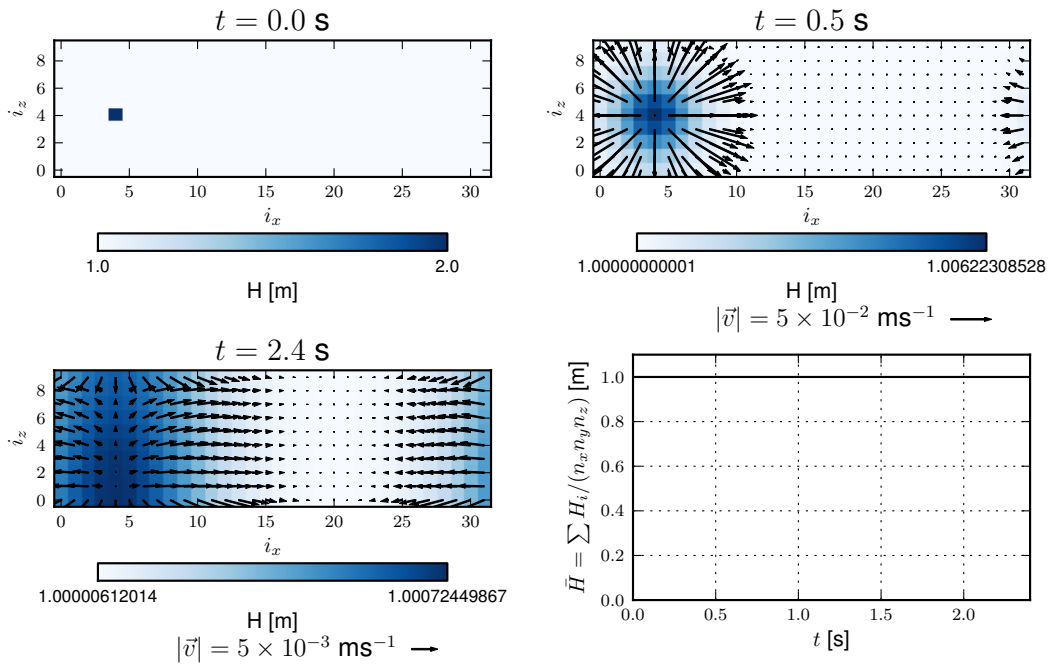

Figure 2: The evolution of the hydraulic heads through time on the (x, z)-plane at $i_y = 4$, and the mean hydraulic head in the three-dimensional grid through time. The fluid (x, z)-velocities are overlain as arrows.

3.1.2 Comparison to an analytical solution of transient flow

In order to validate the transient solutions and the spatial patterns of fluid flow produced by the code, the numerical solver is compared to the analytical Theis solution, describing behavior of a well pumping in a confined aquifer under transient conditions (Theis, 1935; Schwartz and Zhang, 2003).

Originally developed to estimate aquifer hydraulic storativities and transmissivities, Theis' solution assumes a laterally infinite, homogeneous and isotropic aquifer. The aquifer is pumped in a fully penetrating vertical well, pumping with constant discharge, having a infinitesimal diameter. The upper and lower boundaries of the aquifer are impermeable (i.e. no flow). All extracted water comes from the aquifer storage and is discharged instantaneously with the decline in the aquifer hydraulic heads. The Theis solution specifies that the drawdown s, which is defined as the change in hydraulic head $(H_t - H_{t=0})$, can be determined at distance r [m] at time t:

$$s = \frac{Q}{4\pi T} W(u) \quad \text{where} \quad u = \frac{r^2 S}{4Tt} \tag{27}$$

$W(u)$ is the so-called well function containing an infinite series:

$$W(u) = -0.577216 - \ln(u) + u - \frac{u^2}{2!2} + \frac{u^3}{3!3} - \frac{u^4}{4!4} + \dots \tag{28}$$

The drawdown is radially symmetrical, and is termed the *cone of depression*.

The numerical domain has the spatial dimensions $21 \times 21 \times 0.21$ m, discretized into a grid of the dimensions $100 \times 100 \times 1$. The hydraulic conductivity is set to $1 \times 10^{-2}\,\mathrm{m\,s^{-1}}$, the specific storage is set to $8 \times 10^{-3}\,\mathrm{m^{-1}}$, and the initial hydraulic heads are 1 m. Water is extracted from the center cell, producing a discharge of $Q = 1 \times 10^{-4}\,\mathrm{m^3\,s^{-1}}$. The

upper and lower no-flow (Neumann) boundary conditions are implemented by defining the vertical pressure gradients to a constant value of 0. When the analytical values are calculated, the terms with factorial values over 100 are neglected in the well function (eq. 28).

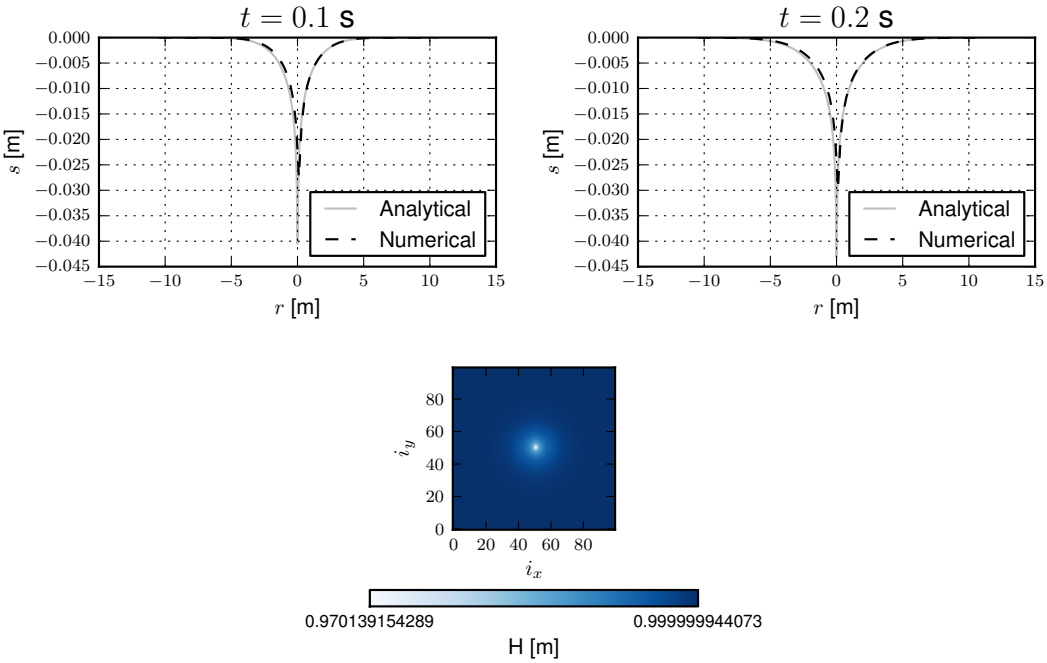

Figure 3: (top) The analytical and hydraulic heads under extraction of fluid volume in the center of the system. The numerical hydraulic heads are read from a line passing through the center of the numerical grid ($(i_z, i_y, i_z) = (1 \ldots 100, 50, 1)$). (bottom) The hydraulic heads at $t = 0.2$ s.

The analytical and numerical solution of the drawdown values are compared at two points in time (fig. 3, top). The solutions are sufficiently similar, validating the transient behavior of the numerical model. The simulated cone of depression is radially symmetrical (fig. 3, bottom), consistent with theory.

3.2 Fluid dynamics during granular deformation

A consolidation experiment is set up to test the effect of the particle deformation upon the fluid dynamics. A flat top wall excerting a constant normal stress is moved downwards into the surface of a particle assemblage. The wall interacts only with the particle phase. The relative movement of particles causes internal porosity fluctuations, which in turn effect the local hydraulic pressure, as well as the local hydraulic conductivity.

Initially, a consolidation experiment was attempted using the cubic sorting cell-based porosity estimation method (fig. 1). The resulting hydraulic pressures and velocities were very large and highly unrealistic. This can be explained by the discontinuous temporal evolution of the cell porosities, owing to the cubic porosity estimation method. These discontinuities cause large values of porosity change during certain time steps, and in turn, a large change in hydraulic pressure (eq. 8). The subsequent experiments are performed using the spherical porosity estimation method, which also result in less spatial variance in the scalar field of porosity (fig. 4).

During the early steps in the consolidation, the particle surface irregular. Two protruding particles (fig. 5, top left) are the first to experience impact with the top wall. They

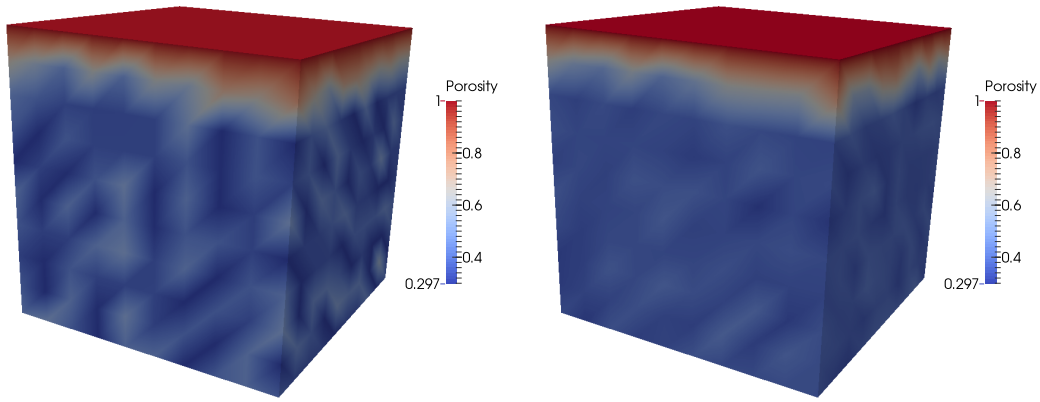

Figure 4: Porosity values at the edges of the fluid grid. (left) Cubic porosity estimation method, (right) Spherical porosity estimation method.

are consequently accelerated downwards, where they impact with other particles. These particles are accelerated mainly in the horizontal direction. The lateral movement away from the initial impacts (fig. 5, top right) causes changes in the porosity (fig. 5, bottom left), which in turn modify the hydraulic pressures (fig 5, bottom right).

3.3 Performance

The performance of the implementation is evaluated by timing the execution time for each of the Darcy routines. The profiling results from the consolidation simulation with 10 000 particles and 100 fluid cells are presented in table 1. The DEM operations are summed into a single entity, and it is clear that these operations are by far the heaviest computational burden. The fluid computations are performed by launching a single GPU processor thread per cell. On the test system, this means that up to 2496 fluid cells may be evaluated simultaneously.

The CUDA implementation of the fluid dynamics utilizes the GPU's global and constant memory (NVIDIA, 2013). Performance is likely to improve by using shared memory when the neighbor cell values are read (Kirk and Hwu, 2010; NVIDIA, 2013), but since the fluid operations are less computationally demanding than the DEM operations, it was decided that the programming effort was better spent elsewhere. The cubic porosity estimation method is by a large margin much faster, occupying 1.41% of the runtime, contrary to the spherical esimtation method occupying 21.5%. The latter method considers particles at a larger distance from the cell center.

4 Outlook

In the current implementation, the effect of particle *velocities* are not transfered to the fluid, and the particles are not affected by the fluid. To correctly approximate the fluid and particle behavior in e.g. fluid-saturated shear experiments, the particle↔fluid coupling must be improved to accommodate for particle velocities, instead of simply particle positions.

In the short time scales simulated by the discrete element method, it is a severe simplification to neglect fluid inertia. Future studies will focus on expanding the fluid implementation to solve the full Navier-Stokes equations. In the reference publications (Shamy and Zeghal, 2005; Zhu and others, 2007), the Navier-Stokes flow of an incompressible

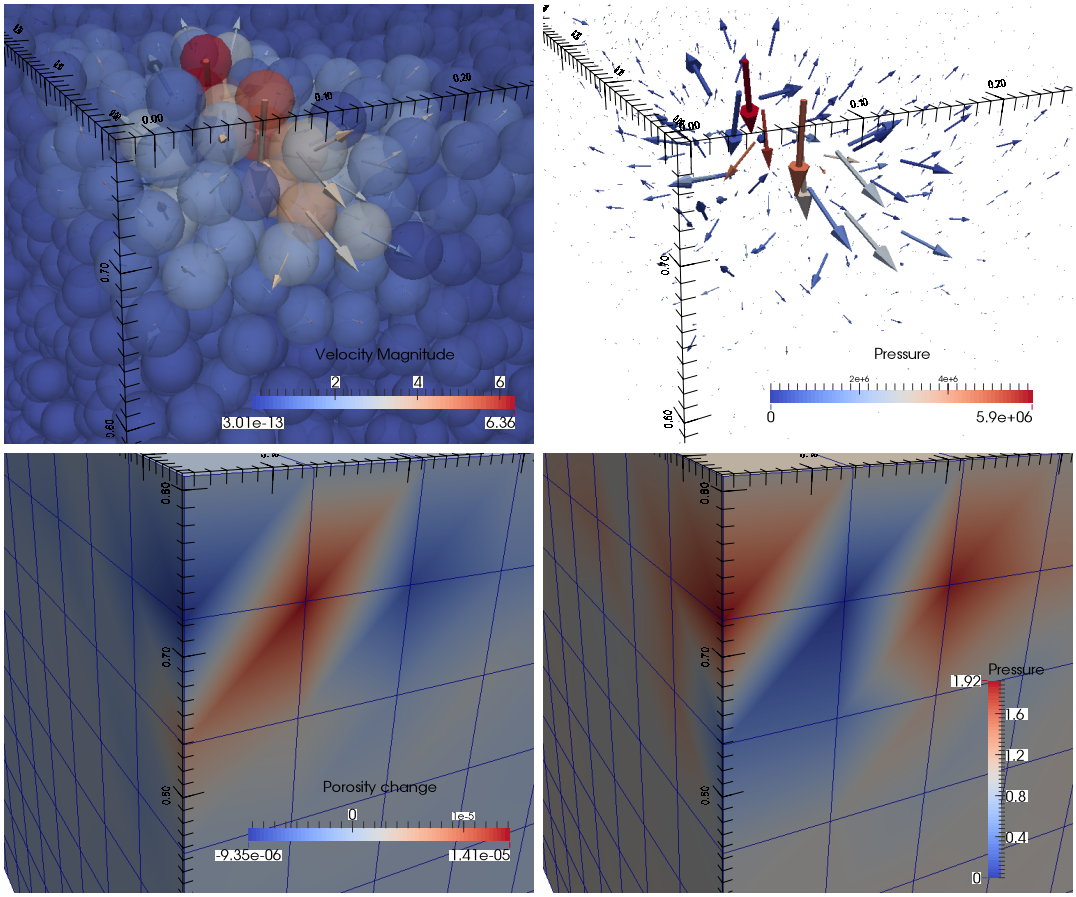

Figure 5: Particle and fluid dynamics during consolidation, visualized from the same view point. (top left) Particles shown as spheres and their linear velocities as arrows, (top right) particle velocity vectors only, colored according to the particle pressure, (bottom left) estimated porosity values, where grid lines intersect at the fluid cell centers, (bottom right) hydraulic pressures.

Kernel	Task	% time
DEM kernels	Discrete Element operations	76.9
`findPorosities`	Find the porosities using eq. 16 and 19	21.5
`findDarcyTransmissivities`	Find the transmissivities using eq. 4, 3, and 21	0.246
`setDarcyGhostNodes`	Copy values from parent to the ghost cells	0.369
`explDarcyStep`	Explicit integration using eq. 22, 23 and 20	0.478
`findDarcyGradients`	Find central difference gradients of H using eq. 26	0.282
`findDarcyVelocities`	Find Darcy velocities using eq. 25	0.275

Table 1: Overview of the time spent in the GPU functions (kernels).

fluid is coupled to the particles by the local porosity value and the averaged velocities:

$$\frac{\partial \phi}{\partial t} + \nabla \cdot (\phi \bar{\vec{v}}_f) = 0 \tag{29}$$

$$\rho_f \left(\frac{\partial (\phi \bar{\vec{v}}_f)}{\partial t} + \nabla \cdot (\phi \bar{\vec{v}}_f \bar{\vec{v}}_f) \right) = -\phi \nabla \bar{p}_f - \bar{\vec{f}}_i + \phi \rho_f \vec{f}_g \tag{30}$$

where $\bar{\vec{v}}_f$ is the cell-averaged fluid velocity, $\bar{p}_f$ is the averaged hydraulic pressure in the cell, $\bar{\vec{f}}_i$ is the averaged fluid–particle interaction force, and $\vec{f}_g$ is the gravitational force. For improving the numerical stability, Shamy and Zeghal (2005) used a staggered grid with pressure nodes in the center, and velocity nodes at the cell boundaries.

The solution will be computed by operator splitting and iteratively solving the system in an explicit scheme proposed by Langtangen and others (2002). Using the above formulation, it will no longer be necessary to rely on the semi-empirical Kozeny-Carman equation (eq. 4), as well as the hydraulic storage which is difficult to constrain. The Navier-Stokes formulation can contrary to the Darcy formulation simulate fluid flow in cells which do not contain particles.

The effect of the fluid flow drag on the in-cell particles and vice versa can be accommodated by using semi-empirical relationships. The drag is caused by particle and fluid velocity differences. Under porosity values less than 0.8, the following relationship can be used (Ergun, 1952; Shamy and Zeghal, 2005):

$$\bar{\vec{f}}_i = \left(150 \frac{\mu_f (1-\phi)^2}{\phi \bar{d}_p^2} + 1.75 \frac{(1-\phi)\rho_f ||\bar{\vec{v}}_f - \bar{\vec{v}}_p||}{\bar{d}_p^2} \right) (\bar{\vec{v}}_f - \bar{\vec{v}}_p) \tag{31}$$

where $\bar{d}_p$ is the mean particle diameter in the fluid cell. For very dilated fluid-particle suspensions ($\phi \geq 0.8$), the fluid–particle interaction force can be approximated by (Wen and Yu, 1966; Shamy and Zeghal, 2005):

$$\bar{\vec{f}}_i = \left(\frac{3}{4} \frac{C_d (1-\phi) \phi^{-2.65} \mu_f \rho_f ||\bar{\vec{v}}_f - \bar{\vec{v}}_p||}{\bar{d}_p} \right) (\bar{\vec{v}}_f - \bar{\vec{v}}_p) \tag{32}$$

where C_d is a drag coefficient determined by the Reynolds number (R_d):

$$C_d = \begin{cases} \frac{24}{R_p}(1 + 0.15 R_p^{0.687}) & \textit{if } R_p < 1000 \\ 0.44 & \textit{if } R_p \geq 1000 \end{cases} \tag{33}$$

The Reynolds number in the fluid-particle mixture is determined by:

$$R_p = \frac{\phi \rho_f \bar{d}_p}{\mu_f} ||\bar{\vec{v}}_f - \bar{\vec{v}}_p|| \tag{34}$$

The interaction force is used to calculate the resulting *drag force* $\vec{f_d}$ on each particle inside the fluid cell:

$$\vec{f_d} = \left(-\nabla \bar{p}_f + \frac{\bar{\vec{f}}_i}{1-\phi} \right) V_p \tag{35}$$

where V_p is the particle volume.

When this two-way coupled implementation with the full equations of momentum is implemented, it will be used to investigate the influence of particle-fluid interaction during subglacial deformation.

5 Conclusion

A simple implementation with a one-way coupling between granular particles and an inter-particle fluid is presented. The fluid flow is simulated in a regular, cubic, spatial discretization by Darcy's law, neglecting fluid inertia, assuming laminar flow and considering the fluid to be incompressible. The hydraulic conductivity is determined by the semi-empirical Kozeny-Carman relationship, which is a function of the local grain diameter and the local porosity. The local porosity is estimated either on the base of the particle center coordinate relative to the cubic cell sides, or based on the intersection of an in-cell spherical volume. The latter method yields continuous porosity values trough time, and the resulting fluid flow stability is improved.

The algorithm is implemented for GPU execution using an explicit scheme. The explicit solution has strict requirements for numerical stability, which is accommodated by using the same, low time step value for both the particle and fluid computations. The performance of the fluid operations is excellent relative to the execution time spent performing the granular operations.

The fluid solver is validated by comparing it to an analytical solution of transient flow in a porous medium. The solver then used to perform a coupled simulation of fluid dynamics under granular deformation.

Finally, future steps are presented for simulating the fluid according to the Navier-Stokes equations, fully coupled to the kinematics of the solid phase.

References

Boek, E.S., C. Hall and P.M.J. Tardy, 2012. Deep bed filtration modelling of formation damage due to particulate invasion from drilling fluids, *Transport in porous media*, **91**(2), 479–508.

Bueler, E., 2012. Numerical modelling of ice sheets, streams, and shelves, Karthaus course notes, `http://github.com/bueler/karthaus`.

Carman, P.C., 1937. Fluid flow through granular beds, *Transactions-Institution of Chemical Engineeres*, **15**, 150–166.

Carman, P.C., 1956. Flow of gases through porous media, Butterworths Scientific Publications London.

Cundall, P.A and O.D.L. Strack, 1979. A discrete numerical model for granular assemblies, *Géotechnique*, **29**, 47–65.

Damsgaard, A., D.L. Egholm, J.A. Piotrowski, S. Tulaczyk, N.K. Larsen and K. Tylmann, 2013. Discrete element modeling of subglacial sediment deformation, *Journal of Geophysical Research - Earth Surface*, accepted.

Ergun, S., 1952. Fluid flow through packed columns, *Chem. Eng. Prog.*, **43**(2), 89–94.

GDR-MiDi, 2004. On dense granular flows, *Eur. Phys. J. E*, **14**, 341–365.

Gerya, Taras, 2010. Introduction to Numerical Geodynamic Modelling, Cambridge University Press, Cambridge.

Harleman, D.R.F., P.F. Mehlhorn and R.R. Rumer, 1963. Dispersion-permeability correlation in porous media, *J. Hydraul. Div. Am. Soc. Civ. Eng*, **89**, 67–85.

Hazen, A., 1911. Discussion of dams on sand formation, *Transactions of the American Society of Civil Engineers*, **73**, 199–221.

Iverson, N.R., T.S. Hooyer and R.W. Baker, 1998. Ring-shear studies of till deformation: Coulomb-plastic behavior and distributed strain in glacier beds, *Journal of Glaciology*, **148**, 634–642.

Jaeger, H.M., S.R. Nagel and R.P. Behringer, 1996. Granular solids, liquids, and gases, *Reviews of Modern Physics*, **68**(4), 1259–1273.

Kirk, D.B. and W-M.W. Hwu, 2010. Programming Massively Parallel Processors, Morgan Kaufmann, Elsevier.

Kozeny, J., 1927. Ueber kapillare leitung des wassers im boden, *Sitzungsber. Akad. Wiss. Wien*, **136**, 271–306.

Krumbein, W.C. and G.D. Monk, 1943. Permeability as a function of the size parameters of unconsolidated sand.

Langtangen, H.P, K.-A. Mardal and R. Winther, 2002. Numerical methods for incompressible viscous flow, *Advances in Water Resources*, **25**(8), 1125–1146.

Li, Y.R. and A. Aydin, 2010. Behavior of rounded granular materials in direct shear: Mechanisms and quantification of fluctuations, *Engineering Geology*, **115**(1-2), 96–104.

Mead, W.J., 1925. The geologic role of dilatancy, *Journal of Geology*, **33**(7), 685–698.

Nedderman, R.M., 1992. Statics and kinematics of granular materials, Cambridge University Press, Cambridge.

Nelson, P.H., 1994. Permeability-porosity relationships in sedimentary rocks, *Log Analyst*, **35**, 38–62.

NVIDIA, 2013. CUDA C Programming Guide, NVIDIA Corporation: Santa Clara, CA, USA, 5.0 ed.

Reynolds, O., 1885. On the dilatancy of media composed of rigid particles in contact, *Phil. Mag*, **20**(5), 46.

Richefeu, V., M.S. El Youssoufi and F. Radjaï, 2006. Shear strength properties of wet granular materials, *Physical Review E*, **73**(5), 051304.

Schwartz, F.W. and H. Zhang, 2003. Fundamentals of ground water.

Shamy, U.E. and M. Zeghal, 2005. Coupled Continuum-Discrete Model for Saturated Granular Soils, *Journal of Engineering Mechanics*, **131**(4), 413–426.

Sonnenborg, T.O. and H.J. Henriksen, 2005. Håndbog i grundvandsmodellering, GEUS, Geological Survey of Denmark and Greenland.

Theis, C.V., 1935. The relation between the lowering of the piezometric surface and the rate and duration of discharge of a well using ground water storage, US Department of the Interior, Geological Survey, Water Resources Division, Ground Water Branch.

Wen, C. and Y. Yu, 1966. Mechanics of fluidization, *Chem. Eng. Prog.*, **62**(62), 100–111.

Zhu, H.P., Z.Y. Zhou, R.Y. Yang and A.B. Yu, 2007. Discrete particle simulation of particulate systems: Theoretical developments, *Chemical Engineering Science*, **62**, 3378–3396.